

Chimera states of phase oscillator populations with nonlocal higher-order couplings

Yonggang Wu(伍勇刚), Huajian Yu(余华健), Zhigang Zheng(郑志刚), and Can Xu(徐灿)

Citation: Chin. Phys. B, 2024, 33 (**4**): 040504. DOI: 10.1088/1674-1056/ad1481
Journal homepage: http://cpb.iphy.ac.cn; http://iopscience.iop.org/cpb

What follows is a list of articles you may be interested in

Quasi-synchronization of fractional-order complex networks with random coupling via quantized control

Hongwei Zhang(张红伟), Ran Cheng(程然), and Dawei Ding(丁大为)
Chin. Phys. B, 2023, 32 (**11**): 110501. DOI: 10.1088/1674-1056/acedf4

Explosive synchronization of multi-layer complex networks based on star connection between layers with delay

Yan-Liang Jin(金彦亮), Qian-Yuan Han(韩钱源), Run-Zhu Guo(郭润珠), Yuan Gao(高塬), and Li-Quan Shen(沈礼权)
Chin. Phys. B, 2023, 32 (**10**): 100507. DOI: 10.1088/1674-1056/acbaf1

Synchronization-desynchronization transitions in networks of circle maps with sinusoidal coupling

Yun Zhai(翟云), Jinghua Xiao(肖井华), and Zhigang Zheng(郑志刚)
Chin. Phys. B, 2023, 32 (**6**): 060505. DOI: 10.1088/1674-1056/acc062

Synchronization of stochastic complex networks with time-delayed coupling

Duolan(朵兰), Linying Xiang(项林英), and Guanrong Chen(陈关荣)
Chin. Phys. B, 2023, 32 (**6**): 060502. DOI: 10.1088/1674-1056/acc44e

Diffusive field coupling-induced synchronization between neural circuits under energy balance

Ya Wang(王亚), Guoping Sun(孙国平), and Guodong Ren(任国栋)
Chin. Phys. B, 2023, 32 (**4**): 040504. DOI: 10.1088/1674-1056/ac7bff

---

Chimera states of phase oscillator populations with nonlocal higher-order couplings

Yonggang Wu(伍勇刚)[1], Huajian Yu(余华健)[1], Zhigang Zheng(郑志刚)[2,†], and Can Xu(徐灿)[2,‡]

[1] *School of Mathematical Sciences, Huaqiao University, Quanzhou* 362021, *China*

[2] *Institute of Systems Science and College of Information Science and Engineering, Huaqiao University, Xiamen* 361021, *China*

(Received 20 September 2023; revised manuscript received 21 November 2023; accepted manuscript online 12 December 2023)

The chimera states underlying many realistic dynamical processes have attracted ample attention in the area of dynamical systems. Here, we generalize the Kuramoto model with nonlocal coupling incorporating higher-order interactions encoded with simplicial complexes. Previous works have shown that higher-order interactions promote coherent states. However, we uncover the fact that the introduced higher-order couplings can significantly enhance the emergence of the incoherent state. Remarkably, we identify that the chimera states arise as a result of multi-attractors in dynamic states. Importantly, we review that the increasing higher-order interactions can significantly shape the emergent probability of chimera states. All the observed results can be well described in terms of the dimension reduction method. This study is a step forward in highlighting the importance of nonlocal higher-order couplings, which might provide control strategies for the occurrence of spatial–temporal patterns in networked systems.

Keywords: synchronization, complex system, coupled oscillators, phase transition

PACS: 05.45.Xt, 89.75.Fb, 89.75.–k **DOI:** 10.1088/1674-1056/ad1481

1. Introduction

Many natural and man-made systems, ranging from physics, biology and chemistry to social sciences, have been modeled as networks of coupled oscillators[1–3] whose components represent dynamical units interacting through links. The most interesting dynamical behavior from coupled networks is the emergence of collective phenomenon, which displays crucial roles underlying a wide range of processes.[4–6]

Over the past few decades, the connectives between different elements in complex systems have mostly been described by pairwise interactions. However, recent studies of complex networks highlighted the potential importance of nonpairwise interactions in addition to pairwise ones.[7–10] It is shown that, in certain realistic networks, such as brain networks, social networks and ecological networks, simple pairwise interactions are not enough to effectively describe the emergent behaviors. Instead, nonpairwise interactions, also known as a peculiar form of higher-order couplings, have been proven to be useful for understanding the intrinsic mechanisms behind the various collective phenomena.[11–14]

Recently, the emergence of symmetry-breaking patterns, called chimera states, has attracted a great deal of attention in the field of dynamical systems.[15–20] Specifically, the chimera state represents a dynamical phenomenon occurring in nonlocal coupling systems in which two different states (the incoherent and the coherent) coexist even when the dynamical units are identical. As a peculiar spatial–temporal pattern, the chimera state has been widely used to account for a plethora of processes of activities observed in brain networks.[21–24]

As a starting point, the authors investigated the spatial–temporal patterns in a system of coupled nonlinear Duffing oscillators, where they identified a phenomenon named similar domain spatial structure.[25] In 2002, a similar phenomenon appearing in coupled phase oscillator systems was reported by Kuramoto and Battogtokh.[26] Furthermore, such collective phenomena were named as chimera-like states by Abrams and Strogatz in 2004.[27] In contrast to the complete synchronized state taking place in the Kuramoto model, the chimera states characterized by the coexistence of drifting and locked oscillators are counterintuitive, which originate from the symmetry-break of the coupled phase oscillators.[28–30,35]

In this paper, we study a nonlocally coupled Kuramoto model with higher-order interactions encoded by a weighted factor. In contrast to previous works, we reveal that the introduced higher-order interactions can significantly increase the probability of the occurrence of the incoherent state. Interestingly, we uncover the fact that the increased higher-order interactions can significantly influence the emergence of chimera states. Specifically, the emergent probability of chimera states exhibits nontrivial dependence on the fraction of higher-order interactions. In particular, we provide a theoretical framework for analyzing the synchronizability of the nonlocal coupling.

The rest of this paper is organized as follows. In Section 2, the dynamical model incorporating higher-order interactions with nonlocal coupling is introduced. In Section 3, we explore the impacts of higher-order interactions on the emer-

†Corresponding author. E-mail: zgzheng@hqu.edu.cn

‡Corresponding author. E-mail: xucan@hqu.edu.cn

© 2024 Chinese Physical Society and IOP Publishing Ltd

gence of chimera states via extensive numerical simulations. In Section 4, we discuss the ability of the synchronization of the observed collective states in terms of matrix analysis theory. In Section 5, we utilize Ott–Antonsen theory to reduce the dynamical system. Finally, conclusions and discussions are presented in Section 6.

2. Dynamical model

In this work, to explore the effect of higher-order interactions on the emergence of chimera states, we consider an N nonlocally coupled identical phase oscillator with 2-body and 3-body interactions. The dynamical equations are as follows:

$$\begin{aligned}\dot{\theta}_i = \omega &+ \frac{\gamma}{N}\sum_{j=1}^{N} G(x_j - x_i)\sin(\theta_j - \theta_i + \alpha) \\ &+ \frac{\nu}{N^2}\sum_{j=1}^{N}\sum_{k=1}^{N} G(x_k + x_j - 2x_i)\sin(\theta_j + \theta_k - 2\theta_i + \beta), \\ i &= 1,\ldots,N, \end{aligned} \tag{1}$$

where $\theta_i(x,t)$ represents the phase of the oscillator at position x at time t. Here the spatial domain is defined as $-\pi \le x \le \pi$ for convenience, thus indicating a ring structure. The positive parameters γ and ν account for the fraction of pairwise (two-body interactions) and nonpairwise (three-body interactions), respectively, with $\gamma + \nu = 1$. The parameters α and β represent the phase delays of two-body interactions and three-body interactions, respectively. For simplicity, we set $\alpha = \beta$, where $0 \le \alpha \le \pi/2$. The model has transform invariance and natural frequency ω does not play any role, thus we set ω to 0 without any loss of generality, which does not change the form of Eq. (1).

The kernel $G(x)$ provides a nonlocal coupling between the oscillators.[26] It is assumed to be even, positive and decaying over the distance between the oscillators in the ring $|x_j - x_i|$ ($|x_k + x_j - 2x_i|$). Specifically, we consider a cosine kernel to account for the periodic boundary condition, which takes the form

$$G(x) = 1 + A\cos x, \tag{2}$$

where $0 \le A \le 1$.

We are interested in the consequences of introducing higher-order interactions in Kuramoto models with phase lags with nonlocal coupling. Before preceding, we restrain the phase variable θ with $0 \le \theta < 2\pi$. As mentioned in previous works, the phase shifts are fixed to achieve the chimera states, i.e., $\alpha = \beta = (\pi/2) - 0.18$. Unless specified otherwise, the initial conditions $\theta_i(x,0)$ are chosen randomly from the interval $[0, 2\pi)$ for each position x. All the numerical methods are implemented using the fourth-order Runge–Kutta integration scheme with fixed time step $\mathrm{d}t = 0.01$.

3. Effect of higher-order interactions

In this section, we investigate the effect of higher-order interactions on dynamical behaviors. For this purpose, three different parametric regimes corresponding to three collective states, namely, the coherent (CO), chimera (CH) and incoherent (IN) states, are distinguished. The consequences of higher-order interactions on the system are illustrated by the probability of the occurrence of these three different dynamical states.

We adopt a classical statistical approach to distinguish three dynamical states,[31] which are calculated as follows:

$$\mathrm{SI} = 1 - \frac{\sum_{m=1}^{\eta} s_m}{\eta}, \tag{3}$$

$$s_m = \Theta[\delta - \sigma(m)], \tag{4}$$

where $\Theta(\cdot)$ is the Heaviside step function and δ is the predefined threshold value. These oscillators are subdivided into η bins of equal length $\beta = N/\eta$, and the local standard deviation $\sigma(m)$ is measured in each bin as

$$\begin{aligned}\sigma(m) &= \left\langle \sqrt{\frac{1}{\beta}\sum_{i=\beta(m-1)+1}^{m\beta} (\Delta\theta_i - \langle\Delta\theta\rangle)^2} \right\rangle_t, \\ m &= 1,2,\ldots,\eta, \end{aligned} \tag{5}$$

where the variable $\Delta\theta_i = \theta_{i+1} - \theta_i$, $i = 1,2,\ldots,N$ denotes the phase difference between the two oscillators, and $\langle\Delta\theta\rangle$ denotes the mean value of all $\Delta\theta$ in the system, as given by $\langle\Delta\theta\rangle = (1/N)\sum_{j=1}^{N}\Delta\theta_j$. The incoherent (IN), coherent (CO), and chimera (CH) regions in the parameter space are characterized by the values $\mathrm{SI} = 0$, $\mathrm{SI} = 1$, and $0 < \mathrm{SI} < 1$ of Eq. (3), respectively.

The emergence of chimera states is influenced by the choice of the initial conditions, whereby we differentiate the dynamical states by the values of Eq. (3) given 1000 initial conditions $\theta(x,0)$ satisfying a random distribution at $[-\pi,\pi]$ intervals, and count the number of occurrences of the three different dynamical states. Using the above method, we can plot the probability diagram about the effect of higher-order interaction fractions on the dynamical states.

First, we observe the effect of higher-order interactions on the dynamical behavior of the system by adjusting the parameters γ and ν. In this case, we can find a phenomenon where the synchronization and desynchronization behaviors coexist. At time $t = 1500$, the phase distribution of the oscillators is shown in Figs. 1(a)–1(c). The spatial–temporal patterns of the observed dynamical behaviors for the chosen parameter values are depicted in Figs. 1(d)–1(f). We can easily see from those plots above that the dynamical behavior shifts as the coefficient γ increases. To see the changes more clearly that occur in the phase oscillators, we can look at Figs. 1(g)–1(i), where individual oscillators belonging to the synchronized cluster are

depicted with red circles and the oscillators plotted with blue dots belong to the incoherent subpopulation which are distributed randomly over the unit circle.

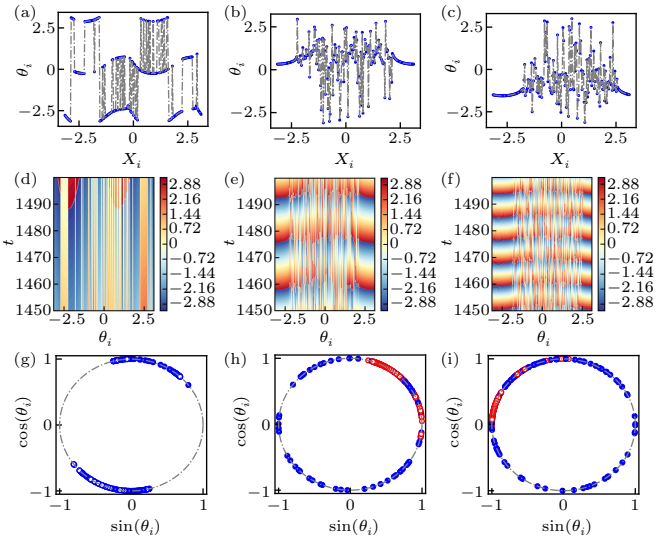


Fig. 1. (a)–(c) Snapshots depict the distribution of phase oscillators at $t = 1500$, where the coefficients γ are 0, 0.5, and 1, respectively (the γ coefficients in the lower panel are arranged as in panels (a)–(c)). We can observe coherent subpopulations and incoherent subpopulations by snapshots. (d)–(f) Spatiotemporal evolution of the non-locally coupled higher-order Kuramoto phase containing the phase lag term. We can observe that the evolutionary behavior of the pure three-body interaction (d) is different from all the others, the system diverges into two populations, and in the two-body interaction or the mixed interaction, we can observe that the system shows a chimera state. (g)–(i) Distribution of all phase oscillators on a unit circle, where synchronous clusters are represented by red circles and incoherent clusters by blue dots. The numerical simulation above is in the parameter $N = 256$ and the initial phases are chosen as $-\pi \le x \le \pi$.

Figure 2 shows a probability plot of the effect of the magnitude of the higher-order interaction proportion on the dynamical states. The impacts of the nonpairwise interactions are varied by adjusting the parameter γ in the plot. It was found that when the coefficient γ is large or small enough, Eq. (1) exists in only two dynamical states, corresponding to the green and purple regions in the plot. In this case, only incoherent and chimera states exist in the green region, and only coherent and chimera states exist in the purple region, and the yellow region indicates the coexistence of the three states. It is observed that the probability of incoherent states increases with the increment of nonpairwise interactions until γ decreases to 0 and the system is almost only in an incoherent state.

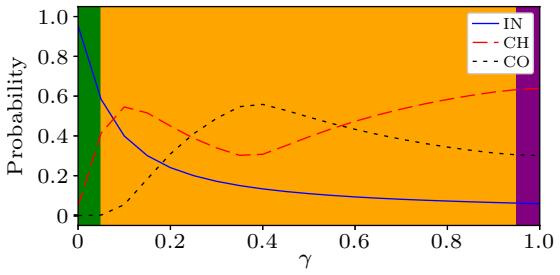


Fig. 2. The change in the probability of the occurrence of the dynamical state is observed by varying the coefficient γ. The probabilities of the three different dynamical states are represented by three different colors. The blue (solid), red (dashed) and green (dotted) colors correspond to incoherent, chimera and coherent dynamics, respectively. Numerical simulation with parameters $\beta = 32$, $N = 256$ and $\delta = 0.38$.

4. Analysis of synchronizability

In this section, we study the effect of higher order interactions on the synchronization capacity.[10,32] For this purpose, we present the Jacobi matrix[33,34] of Eq. (1) as follows:

$$
\begin{aligned}
J_{ij} &= \frac{\partial \dot{\theta}_i}{\partial \theta_j} \\
&= \frac{\partial}{\partial \theta_j}\left[\omega + \left[\left[1 + A\cos\left(x_k - x_i\right)\right]\frac{\gamma}{N}\sum_{k=1}^{N}\sin\left(\theta_k - \theta_i + \alpha\right) + \frac{1-\gamma}{N^2}\sum_{k=1}^{N}\sum_{l=1}^{N}\left[1 + A\cos\left(x_k + x_l - 2x_i\right)\right]\sin\left(\theta_k + \theta_l - 2\theta_i + \alpha\right)\right]\right] \\
&= \frac{\gamma}{N}\sum_{k=1}^{N}\frac{\partial\left[1 + A\cos\left(x_k - x_i\right)\right]\sin\left(\theta_k - \theta_i + \alpha\right)}{\partial \theta_j} + \frac{1-\gamma}{N^2}\sum_{k=1}^{N}\sum_{l=1}^{N}\frac{\partial\left[1 + A\cos\left(x_k + x_l - 2x_i\right)\right]\sin\left(\theta_k + \theta_l - 2\theta_i + \alpha\right)}{\partial \theta_j} \\
&= -\frac{\gamma}{N}\sum_{k=1}^{N}\left[1 + A\cos\left(x_k - x_i\right)\right]\cos\left(\theta_k - \theta_i + \alpha\right)\delta_{ij} + \frac{\gamma}{N}\left[1 + A\cos\left(x_k - x_i\right)\right]\cos\left(\theta_k - \theta_i + \alpha\right) - \frac{2-2\gamma}{N^2} \\
&\quad \times \sum_{k=1}^{N}\sum_{l=1}^{N}\left[1 + A\cos\left(x_k + x_l - 2x_i\right)\right]\cos\left(\theta_k + \theta_l - 2\theta_i + \alpha\right)\delta_{ij} + \frac{2-2\gamma}{N^2}\left[1 + A\cos\left(x_k + x_l - 2x_i\right)\right]\cos\left(\theta_k + \theta_l - 2\theta_i + \alpha\right). \quad (6)
\end{aligned}
$$

The synchronization state, i.e., $\theta_i = \theta_j$ for all $i \neq j$, is a solution of Eq. (1). Since each phase oscillator is identical, equation (6) is only affected by the spatial position, phase lag and the γ coefficient, but we are solely talking about the effect of higher-order interactions. Therefore, we do not discuss the effect of phase lag on the synchronization capability. Thus, for the synchronized state, the Jacobian is expressed as

$$
\begin{aligned}
J_{ij} \;=\; & -\frac{\gamma}{N}\sum_{k=1}^{N}\left[1 + A\cos\left(x_k - x_i\right)\right]\cos\left(\alpha\right)\delta_{ij} + \frac{\gamma}{N}\left[1 + A\cos\left(x_k - x_i\right)\right]\cos\left(\alpha\right) \\
& -\frac{2-2\gamma}{N^2}\sum_{k=1}^{N}\sum_{l=1}^{N}\left[1 + A\cos\left(x_k + x_l - 2x_i\right)\right]\cos\left(\alpha\right)\delta_{ij} + \frac{2-2\gamma}{N^2}\left[1 + A\cos\left(x_k + x_l - 2x_i\right)\right]\cos\left(\alpha\right). \quad (7)
\end{aligned}
$$

It can be easily seen that there is a zero eigenvalue. We further sort all the eigenvalues of the Jacobian Eq. (7) as $0=\lambda_1\geq\lambda_2\cdots\geq\lambda_{N-1}\geq\lambda_N$. The second largest eigenvalue determines the stability of the system, and the larger the absolute value of the second largest eigenvalue, the faster the recovery from perturbation, i.e., the better the synchronization capability.

We start by showing the effect of γ (the proportion of the coupling strength assigned to the second-order interaction) on λ_2. From Fig. 3, we can find that the second largest eigenvalue λ_2 increases with increasing γ, i.e., the synchronization capacity decreases. This is physically reasonable because higher-order interactions allow more nodes to exchange information simultaneously, thus permitting more efficient communication and ultimately leading to improved synchronization performance.

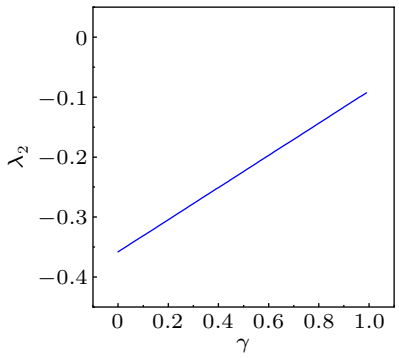


Fig. 3. The second largest eigenvalue λ_2 of the Jacobi matrix is plotted against γ. The coupling changes from second-order-only ($\gamma=0$) to first-order-only ($\gamma=1$) as γ increases. Numerical simulation $N=256$.

5. Ott–Antonsen approach

We explore some theoretical insights into the observed chimera dynamics by using the Ott–Antonsen approach[36,37] in the thermodynamic limit $N\to\infty$. To simplify Eq. (1), we need to introduce two local order parameters as follows:

$$R_{1i}=\frac{1}{N}\sum_{j=1}^{N}[1+A\cos(x_j-x_i)]\,\mathrm{e}^{\mathrm{i}\theta_j}, \tag{8}$$

$$R_{2i}=\frac{1}{N^2}\sum_{j=1}^{N}\sum_{k=1}^{N}[1+A\cos(x_k+x_j-2x_i)]\,\mathrm{e}^{\mathrm{i}(\theta_k+\theta_j)}. \tag{9}$$

Using complex order parameters R_{1i} and R_{2i}, equation (1) can be rewritten as

$$\dot{\theta}_i=\omega+\frac{1}{2\mathrm{i}}(H_i\,\mathrm{e}^{-\mathrm{i}\theta_i}-H_i^*\,\mathrm{e}^{\mathrm{i}\theta_i}), \tag{10}$$

where $H_i=\gamma R_{1i}\,\mathrm{e}^{\mathrm{i}\alpha}+(1-\gamma)R_{2i}\,\mathrm{e}^{-\mathrm{i}\theta_i+\mathrm{i}\beta}$ and H_i^* denotes the complex conjugate.

To determine the degree of coherence between neighboring oscillators, we define the local complex order parameter as the combination of R_{1i} and R_{2i}

$$R_i=\frac{R_{1i}+R_{2i}}{2}, \tag{11}$$

where a larger $|R_i|$ represents a higher degree of coherence between the oscillators.

In the continuum limit, the state of the system can be represented by the probability density function $f(x,\theta,t)$, which gives the proportion of oscillators whose phases lie between θ and $\theta+\mathrm{d}\theta$ at time t. Since the number of oscillators in the system is conserved, the distribution function $f(x,\theta,t)$ satisfies the continuity equation

$$\frac{\partial f}{\partial t}+\frac{\partial(fv)}{\partial\theta}=0. \tag{12}$$

Here, $v=\dot{\theta}_i$ is given in Eq. (10), and $f(x,\theta,t)$ can be expanded by the Fourier series as $f(x,\theta,t)=(1/2\pi)[1+\sum_{n=1}^{\infty}(\{h(x,t)\}^n\,\mathrm{e}^{\mathrm{i}n\theta}+\{h^*(x,t)\}^n\,\mathrm{e}^{-\mathrm{i}n\theta})]$. Substituting f into Eq. (12), we obtain the time evolution of the variable $h(x_i,t)$ associated with the oscillator at position x_i as

$$\begin{aligned}\frac{\partial h(x_i,t)}{\partial t}=&-\mathrm{i}\omega h(x_i)+\frac{1}{2}\Big[\gamma\left(R_{1i}^*\,\mathrm{e}^{-\mathrm{i}\alpha}-R_{1i}\,\mathrm{e}^{\mathrm{i}\alpha}h(x_i,t)^2\right)\\&+(1-\gamma)\left(R_{2i}^*\,\mathrm{e}^{-\mathrm{i}\beta}h(x_i,t)^{-1}-R_{2i}\,\mathrm{e}^{\mathrm{i}\beta}h(x_i,t)^3\right)\Big].\end{aligned} \tag{13}$$

In addition, the order parameters R_{1i} and R_{2i} can also be derived using $h(x_i,t)$ as

$$\begin{aligned}R_{1i}&=\frac{1}{N}\sum_{j=1}^{N}[1+A\cos(x_j-x_i)]\,\mathrm{e}^{\mathrm{i}\theta_j}\\&=\frac{1}{N}\sum_{j=1}^{N}[1+A\cos(x_j-x_i)]\int_0^{2\pi}f(x,\theta_j,t)\,\mathrm{e}^{\mathrm{i}\theta_j}\,\mathrm{d}\theta_j\\&=\frac{1}{N}\sum_{j=1}^{N}[1+A\cos(x_j-x_i)]\,h^*(x_j,t),\end{aligned} \tag{14}$$

$$\begin{aligned}R_{2i}&=\frac{1}{N^2}\sum_{j=1}^{N}\sum_{k=1}^{N}(1+A\cos(x_k+x_j-2x_i))\,\mathrm{e}^{\mathrm{i}(\theta_j+\theta_k)}\\&=\frac{1}{N^2}\sum_{j=1}^{N}\sum_{k=1}^{N}(1+A\cos(x_k+x_j-2x_i))\\&\quad\times\int_0^{2\pi}f(x,\theta_j,t)\,\mathrm{e}^{\mathrm{i}\theta_j}\,\mathrm{d}\theta_j\int_0^{2\pi}f(x,\theta_k,t)\,\mathrm{e}^{\mathrm{i}\theta_k}\,\mathrm{d}\theta_k\\&=\frac{1}{N^2}\sum_{j=1}^{N}\sum_{k=1}^{N}[1+A\cos(x_k+x_j-2x_i)]\,h^*(x_j,t)\,h^*(x_k,t).\end{aligned} \tag{15}$$

The function $h(x_i,t)$ and the order parameters R_{1i},R_{2i} can be obtained by using Eqs. (13)–(15). Therein, the initial value of $h(x_i,0)$ can be given by the numerically simulated order parameter R_i.

As shown in Fig. 4, we can see the parameter plots for $\gamma=0,0.5,1$ with different coefficients which correspond to three rows of plots. On the other hand, the columns in the figures correspond to the instantaneous phase diagram of the oscillator at $t=1500$, the spatiotemporal evolution of the oscillators, and the spatiotemporal evolution of the order parameters, respectively.

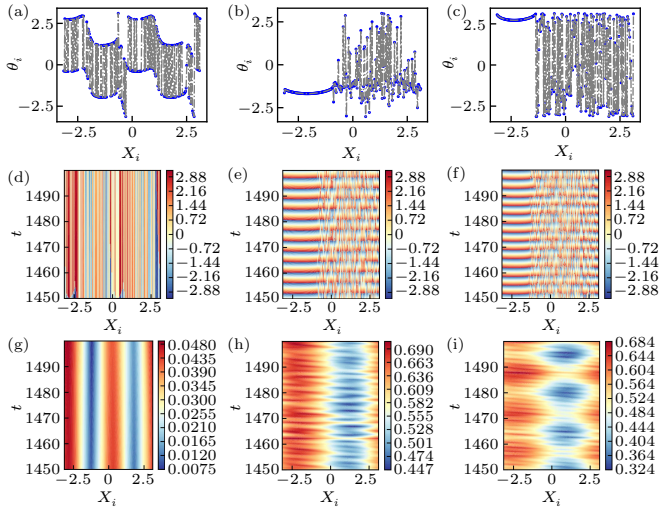


Fig. 4. (a)–(f) The same as in Fig. 2. (g)–(i) Spatiotemporal transformation plots represent the extent of coherence in the evolution of dynamical equations.

Figure 5 illustrates the plots at a coefficient of $\gamma = 0.5$. In Fig. 5(a), the instantaneous phase plot at $t = 1500$ is shown; in Fig. 5(b), the order parameter plot corresponding to Fig. 5(a) is shown; Fig. 5(c) shows the spatiotemporal evolution of the order parameters.

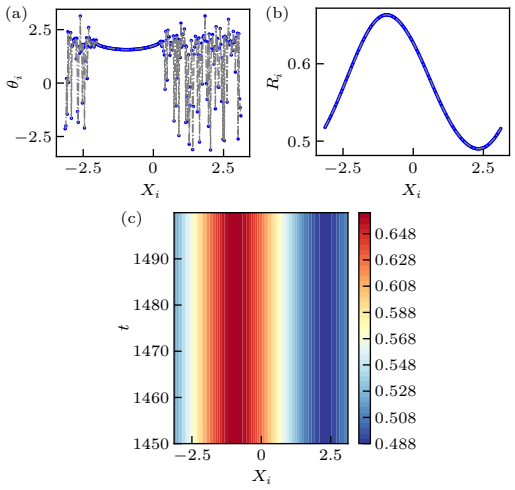


Fig. 5. (a) Snapshots of the chimera state dynamical equation with coefficient $\gamma = 0.5$. (b) The $|R_i|$ image at a particular time is calculated by the OA approach using Eqs. (13)–(15). (c) Spatiotemporal variation of the order parameter amplitude $|R_i|$ computed directly from the numerical simulations.

6. Conclusions

In summary, there has been growing interest in exploring synchronized dynamics in networks with nonpairwise interactions. Chimera states, serving as a most fascinating phenomena, have attracted great attention in scientific communities. In this work, we have investigated chimera states in the generalized Kuramoto model by taking into account nonlocal couplings and higher-order interactions, simultaneously.

In previous works,[9,13] it has been shown that higher-order interactions favor synchronization transitions, i.e., the coherent states are significantly improved compared with only pairwise interactions. Interestingly, we identified that the two effects (nonlocal and nonpairwise) combine together to shape the collective dynamics of the system. Specifically, we uncovered that the nonlocal higher-order couplings give rise to multiple chimera states in addition to a stable asynchronious state. By introducing a standard statistical method, we showed that the probability of the occurrence of the incoherent state is increased with the increment of the fraction of higher-order interactions. However, the probability of the emergence of chimera states exhibits an irregular dependence on the weight of higher-order interactions. The main reason why our work differs from previous work[9,13] is that a different coupling approach has been adopted. Previous work[9,13] adjusts the coupling strength through a coefficient K, whereas our work relates the coupling strength to the position of the oscillator and modulates it via the positional relationship.

In terms of matrix theory, we argued that the synchronizability of the system is remarkably enhanced with the increasing of higher-order interactions. We find that improved synchronization capability does not necessarily mean a higher probability of the system reaching a synchronized state. Furthermore, Ott–Antonsen theory is used to capture the low-dimensional macroscopic dynamics that matches the numerical simulation well. Our work has thus provided insights for understanding the various pattern formations in networks with nonlocal and higher-order interactions.

Acknowledgments

Project supported by the National Natural Science Foundation of China (Grants Nos. 12375031 and 11905068), the Natural Science Foundation of Fujian Province, China (Grant No. 2023J01113), and the Scientific Research Funds of Huaqiao University (Grant No. ZQN-810).

References

[1] Boccaletti S, Latora V, Moreno Y, Chavez M and Hwang D U 2006 *Phys. Rep.* **424** 175
[2] Gupta S, Campa A and Ruffo S 2014 *J. Stat. Mech.: Theory Exp.* **2014** R08001
[3] Stankovski T, Pereira T, Mcclintock P and Stefanovska A 2017 *Rev. Mod. Phys.* **4** 045001
[4] Strogatz S H 2000 *Physica D* **143** 1
[5] Acebrón J A, Bonilla L L, Vicente C J P, Ritort F and Spigler R 2005 *Rev. Mod. Phys* **77** 137
[6] Pikovsky A and Rosenblum M 2015 *Chaos* **25** 097616
[7] Ghorbanchian R, Restrepo J G, Torres J J and Bianconi G 2021 *Commun. Phys.* **4** 120
[8] Wang X, Zheng Z G and Xu C 2021 *Phys. Rev. E* **104** 054208
[9] Xu C, Zhai Y, Wu Y G, Zheng Z G and Guan S G 2023 *Chaos Solitons Fractals* **170** 113343
[10] Zhang Y Z, Lucas M and Battiston F 2023 *Nat. Commun.* **14** 1605
[11] Gong C C and Pikovsky A 2019 *Phys. Rev. E* **100** 062210
[12] Lucas M, Cencetti G and Battiston F 2020 *Phys. Rev. Res.* **2** 033410
[13] Millán A P, Torres J J and Bianconi G 2020 *Phys. Rev. Lett.* **124** 218301

[14] Skardal P S and Arenas A 2020 *Commun. Phys.* **3** 218
[15] Yao N and Zheng Z G 2016 *Int. J. Mod. Phys. B* **30** 1630002
[16] Rodrigues F A, Peron T K D, Ji P and Kurths J 2016 *Phys. Rep.* **610** 1
[17] Kundu S and Ghosh D 2022 *Phys. Rev. E* **105** L042202
[18] Hagerstrom A M, Murphy T E, Roy R, Hovel P, Omelchenko I and Schöll E 2012 *Nat. Phys.* **8** 658
[19] Tinsley M R, Nkomo S and Showalter K 2012 *Nat. Phys.* **8** 662
[20] Nkomo S, Tinsley M R and Showalter K 2013 *Phys. Rev. Lett.* **110** 244102
[21] Laing C R 2011 *Physica D* **240** 1960
[22] Wimmer K, Nykamp D Q, Constantinidis C and Compte A 2014 *Nat. Neurosci.* **17** 431
[23] Tognoli E and Scott Kelso J A 2014 *Neuron* **81** 35
[24] Laing C R and Chow C C 2001 *Neur. Comput.* **13** 1473
[25] Umberger D K, Grebogi C, Ott E and Afeyan B 1989 *Phys. Rev. A* **39** 4835
[26] Kuramoto Y and Battogtokh D 2002 arXiv:cond-mat/0210694 [cond-mat.stat-mech]
[27] Abrams D M and Strogatz S H 2004 *Phys. Rev. Lett.* **93** 174102
[28] Abrams D M and Strogatz S H 2006 *Int. J. Bifurc. Chaos* **16** 21
[29] Abrams D M, Mirollo R, Strogatz S H and Wiley D A 2008 *Phys. Rev. Lett.* **101** 084103
[30] Martens E A, Laing C R and Strogatz S H 2010 *Phys. Rev. Lett.* **104** 044101
[31] Omel'chenko O E 2013 *Nonlinearity* **26** 2469
[32] Gopal R, Chandrasekar V K, Venkatesan A and Lakshmanan M 2014 *Phys. Rev. E* **89** 052914
[33] Tang Y, Shi D H and Lü L Y 2022 *Commun. Phys.* **5** 96
[34] Carlu M, Ginelli F and Politi A 2018 *Phys. Rev. E* **97** 012203
[35] Omel'chenko O E, Wolfrum M and Maistrenko Y L 2010 *Phys. Rev. E* **81** 065201
[36] Ott E and Antonsen T M 2008 *Chaos* **18** 037113
[37] Ott E and Antonsen T M 2009 *Chaos* **19** 023117